CAAI Transactions on Intelligence Technology

WILEY

The Institution of Engineering and Technology

ORIGINAL RESEARCH OPEN ACCESS

Training-Efficient Personalised Knee Joint Moment Estimation via an Incremental Broad Learning System

Guoyu Zuo[1,2] | Minghui Zhang[1,2] | Jingwei Ren[3] | Qifei Wu[1,2] | Jiaxin Li[3] | Jianyu Chen[3] | Chengyu Qiao[3] | Shuangyue Yu[1,2]

[1]School of Artificial Intelligence, Beijing University of Technology, Beijing, China | [2]Beijing Key Laboratory of Computing Intelligence and Intelligent Systems, Beijing, China | [3]Hangzhou Zhiyuan Research Institute Co. Ltd, Hangzhou, China

Correspondence: Shuangyue Yu (yushuangyue@bjut.edu.cn)

Received: 5 January 2026 | **Revised:** 3 June 2026 | **Accepted:** 1 July 2026

Keywords: incremental broad learning system | joint torque estimation | knee joint moment | wearable robots

ABSTRACT

Knee joint moment estimation is a critical component in biomechanical analysis, with profound implications for rehabilitation assessment and the development of assistive devices like exoskeletons. However, existing data-driven approaches often rely on highly complex network architectures in pursuit of high accuracy, resulting in inherently inefficient training procedures. Furthermore, incorporating new subject-specific data typically requires retraining the entire model, which substantially increases computational cost. These limitations make it challenging for current data-driven methods to achieve personalised knee joint moment estimation. To address this challenge, this paper proposes a novel framework based on an Incremental Broad Learning System (IBLS) that can achieve efficient model training through a flattened network architecture and an analytical ridge regression solver. More importantly, it integrates an incremental learning algorithm that enables rapid model updates using only newly acquired subject-specific data, eliminating the need for costly full retraining. These capabilities collectively make efficient personalised knee joint moment estimation feasible. Extensive experiments on Dataset A and Dataset B demonstrate that our method achieves higher prediction accuracy compared to standard baselines (ANN and LSTM). Furthermore, our approach exhibits competitive performance when compared with advanced deep learning architectures (Transformer and TCN-LSTM). Notably, the training efficiency is significantly enhanced: the training time required by our method is approximately 30% of that for ANN, 7.5% for LSTM, and only 3.5% for both the Transformer and TCN-LSTM. Further experimental evidence indicates that incorporating incremental learning provides an additional 60% reduction in training time relative to full retraining, without sacrificing prediction accuracy. In addition, we systematically identify optimal Inertial Measurement Unit (IMU) configurations that balance accuracy with practical wearability, providing actionable guidelines for implementation. This work provides an efficient, accurate, and personalised solution for knee joint moment estimation, paving the way for the development of adaptive and efficient wearable robotic systems.

1 | Introduction

The accurate estimation of knee joint moments is fundamental to decoding human locomotion, playing a pivotal role in sports science [1], rehabilitation progress monitoring [2–4], and the moment control of lower-limb exoskeletons [5–10]. Traditional inverse dynamics using optical motion capture systems combined with force plates remains the widely accepted gold standard for quantifying joint moments [11, 12]. However, optical motion capture systems and force plates are expensive, bulky,

This is an open access article under the terms of the Creative Commons Attribution-NonCommercial-NoDerivs License, which permits use and distribution in any medium, provided the original work is properly cited, the use is non-commercial and no modifications or adaptations are made.

© 2026 The Author(s). *CAAI Transactions on Intelligence Technology* published by John Wiley & Sons Ltd on behalf of The Institution of Engineering and Technology and Chongqing University of Technology.

and require highly controlled laboratory environments. The reliance on extensive marker placement, system calibration, and post-processing further limits their feasibility for data collection and robot control.

To overcome these limitations, recent studies have increasingly explored data-driven approaches based on wearable sensors. These methods estimate joint moments directly from kinematic or physiological signals using lightweight, easily deployable devices such as IMUs, EMG sensors, and instrumented insoles. This approach eliminates the need for force plates or optical systems, thereby greatly enhancing portability and practical applicability. Early studies primarily employed classical machine learning techniques such as Support Vector Machines (SVMs) and ANNs [13–17]. With the advancement of deep learning, recurrent neural architectures became dominant, among which LSTM networks have played a central role due to their strong capability in capturing the temporal dynamics of gait [18–21]. Subsequently, more sophisticated architectures were introduced, such as Graph Convolutional Networks (GCNs) for explicitly representing skeletal topology [22] and transformer models for capturing long-range temporal dependencies [23–27]. Through increased architectural complexity, these methods have progressively pushed the upper limits of joint moment prediction accuracy.

Although existing data-driven approaches have substantially improved the accuracy of knee joint moment estimation, they still fail to support efficient personalised prediction. This limitation arises because many models rely on highly complex deep network architectures, whose reliance on multilayer backpropagation leads to inherently low training efficiency. More critically, when incorporating new subject-specific data, these models typically require merging the additional samples with the original training set and performing a full retraining cycle, resulting in considerable computational overhead. Therefore, a practical method achieving both high accuracy and computational efficiency is needed for personalised knee joint moment estimation.

To meet the need for efficient personalised knee joint moment prediction, this paper introduces a novel framework based on an Incremental Broad Learning System (IBLS) [28–34]. The IBLS is strategically chosen for its unique combination of a flat network structure, which enables extreme training efficiency, and a built-in incremental learning capability, which facilitates seamless personalisation. Specifically, its flat network structure, coupled with a ridge regression-based analytical solution for output weights, fundamentally bypasses the need for gradient-based iterative optimisation. This leads to a substantial reduction in training time, without sacrificing representational power. Moreover, its inherent incremental learning capability provides a principled and efficient mechanism for personalisation. It allows the model to be rapidly calibrated for a new subject by updating only the necessary parameters with the new data, effectively adapting a general model to an individual's unique biomechanics without the prohibitive cost and delay of full retraining. This 'general model + incremental fine-tuning' paradigm is particularly suited for applications like exoskeletons, where rapid adaptation to individual users is crucial.

To explicitly articulate the primary methodological novelty beyond existing BLS or incremental learning literature, this research demonstrates an innovation in its application context. Prior BLS-based research has predominantly applied BLS-related methods to industrial scenarios. For instance, Cao et al. [35] and Xu et al. [36] utilised these methods for remaining useful life estimation, while Zhu et al. [37] and Xu et al. [38] employed them for condition recognition for energy pipeline safety and online fault diagnosis of rotating machinery, respectively. To date, no prior BLS-based biomechanical or wearable-sensor studies have applied the BLS to the field of human joint moment prediction. Compared to industrial applications, human moment exhibits a higher degree of randomness and individual variability, which directly necessitates our targeted personalisation strategy.

The main contributions of this work are threefold:

1. A personalised estimation framework: We developed and validated an IBLS-based framework for knee joint moment estimation that substantially reduces the computational cost of model training while maintaining predictive accuracy, thereby enabling practical personalisation of knee joint moment prediction.
2. Systematic sensor configuration optimisation: We conduct a comprehensive analysis of IMU placements and temporal window sizes, identifying optimal configurations that balance estimation accuracy with practical constraints like wearability and cost, providing clear design guidelines for real-world systems.
3. Extensive experimental validation: We rigorously evaluate our method on two public datasets across three locomotion modes (level walking, stair ascent, and descent), demonstrating estimation accuracy comparable to existing methods (ANN, LSTM, Transformer, and TCN-LSTM) while achieving superior training efficiency. Moreover, further experimental results show that incorporating incremental learning yields an additional notable decrease in training time relative to full retraining, while maintaining comparable prediction accuracy.

The remainder of this paper is organised as follows: Section 2 details the methodology of the IBLS and its application to knee moment estimation. Section 3 describes the experimental setup and datasets and presents the results. Section 4 provides a discussion. Section 5 concludes the paper.

2 | Method

This section first provides a formal definition of the core problem, followed by an introduction to the topological architecture of the IBLS, including the node construction process, the weight computation algorithm, and the dynamic update strategy for incremental streaming data. Finally, an incremental learning framework for personalised knee joint moment prediction is established. The core principles are illustrated in Figure 1.

2.1 | Problem Description

The primary objective of this study is to address the challenges of low computational efficiency and the lack of model personalisation in data-driven knee joint moment estimation.

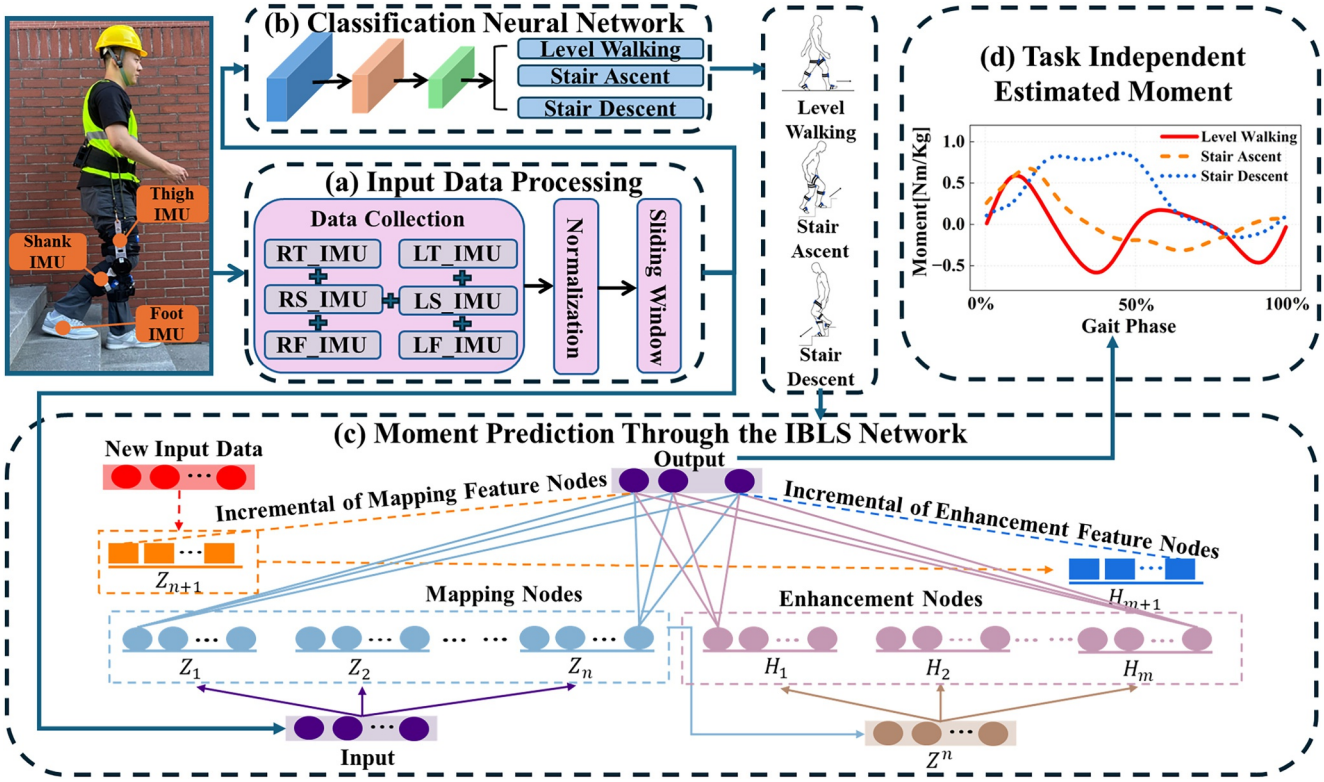


FIGURE 1 | Schematic of the knee joint moment estimation framework based on the Incremental Broad Learning System (IBLS). (a) Input data processing: Raw signals consist of orientation data collected from six IMUs placed on both thighs, shanks, and feet. Temporal features are extracted using a sliding window and used as inputs for both gait classification and moment prediction. (b) Classification neural network: The classification network identifies the current locomotion mode (level walking [LW], stair ascent [SA], and stair descent [SD]), which determines the corresponding moment prediction subnet to be activated. (c) Moment prediction through the IBLS network: Each locomotion mode is associated with a dedicated flattened IBLS prediction network. The model supports incremental learning, enabling efficient parameter updates with new data while producing accurate knee joint moment estimations for the selected gait.

Traditional deep learning models require long training times and offer limited adaptability to individual users. Our goal is to develop a framework that achieves exceptionally efficient training while enabling personalisation with minimal computational overhead. Owing to its architectural characteristics that directly confront these challenges, the IBLS is strategically adopted as the foundation of our framework.

The proposed IBLS serves as an alternative to traditional modelling methods and deep learning approaches for knee moment prediction during level walking, stair ascent, and descent. This methodology establishes nonlinear mappings between multipositionally configured IMU angular data and knee moments. Formally, given initial training data $\{(X, Y)|X \in \mathbb{R}^{N\times d}, Y \in \mathbb{R}^{N\times c}\}$ with N denoting sample cardinality, d representing the number of joint angles processed by the IMU ($d \in [2, 6]$ adopted herein), and $c = 1$ corresponding to the univariate regression task (knee moment), the base mapping ψ satisfies $Y_{\text{Predict}} = \psi(X_{\text{Test}})$. Upon acquiring new data streams, the augmented training data is denoted as $\{(X_a, Y_a)|X_a \in \mathbb{R}^{M\times d}, Y_a \in \mathbb{R}^{M\times c}\}$ with M representing the cardinality of newly incorporated samples; the incremental learning algorithm enhances prediction accuracy by updating the model parameter space to ψ^*, yielding refined predictions $Y^*_{\text{Predict}} = \psi^*(X_{\text{Test}})$. This iterative refinement progressively aligns model predictions with individual-specific knee moment trajectories under actual usage conditions. The complete procedure is detailed in Algorithm 1, with an explanation of the variables provided in the subsequent section.

ALGORITHM 1 | Incremental broad learning system.

Input: Original data $\{(X, Y)|X \in \mathbb{R}^{N\times d}, Y \in \mathbb{R}^{N\times c}\}$
Initialize IBLS with n mapping nodes and m enhancement nodes;
for $i = 1; i \le n$ **do**
  Generate W_{ei} and β_{ei} ;
  Calculate Z_i by Eq. (1);
end
  Set the mapping nodes group $Z^n \triangleq [Z_1, Z_2, \dots, Z_n]$;
for $j = 1; j \le m$ **do**
  Generate W_{hj} and β_{hj};
  Calculate H_j by Eq. (2) ;
end
Set the enhancement nodes group $H^m \triangleq [H_1, H_2, \dots, H_m]$;
Set $A^m_n \triangleq [Z^n \mid H^m]$;
Calculate W^m_n by Eq. (5);
While the new data $\{(X_a, Y_a)|X \in \mathbb{R}^{M\times d}, Y \in \mathbb{R}^{M\times c}\}$ is obtained **do**
  Calculate Z_{li} by Eq. (6);
  Update $Z^n_l \triangleq [Z_{l1}, Z_{l2}, \dots, Z_{ln}]$;
  Calculate H_{lj} by Eq. (7);
  Update $H^m_l \triangleq [H_{l1}, H_{l2}, \dots, H_{lm}]$;
  Set $A^m_{ln} \triangleq [Z^n_l \mid H^m_l]$
  Update $(A^m_n)^* = \begin{bmatrix} A^m_n \\ (A^m_{ln})^T \end{bmatrix}$ and calculate the pseudoinverse of $(A^m_n)^*$ by Eq. (8);
  Update $(W^m_n)^*$ by Eq. (10);
end
Output: $Y = A^m_n W^m_n$ or $Y = (A^m_n)^*(W^m_n)^*$

2.2 | Structure of the Incremental Broad Learning System

The IBLS is uniquely suited to meet the dual demands of efficiency and personalisation in biomechanical estimation. Its flat network structure is key to computational efficiency. IBLS employs a single-layer pseudoinverse to achieve highly efficient training. Furthermore, its incremental learning mechanism directly integrates new data into the existing model, notably reducing computational costs and making personalisation practically feasible. This combination of a fast-initialisation flat structure and an efficient update mechanism makes IBLS an ideal solution for our objectives.

2.2.1 | *The Network Structure of IBLS*

The IBLS, as a lightweight extension of Random Vector Functional-Link Neural Networks (RVFLNN), employs a flattened architecture comprising feature nodes (performing linear transformations) and enhancement nodes (achieving nonlinear mappings), with detailed topology illustrated in Figure 1.

Given training data $\{(X, Y)|X \in \mathbb{R}^{N\times d}, Y \in \mathbb{R}^{N\times c}\}$ where N denotes sample cardinality, d feature dimensionality, and c output dimensionality, the initial IBLS configuration contains n groups of mapping feature nodes and m groups of enhancement feature nodes, each with p and q neurons, respectively. The output of the ith group of mapping feature nodes is computed as:

$$Z_i = \phi_i(XW_{ei} + \beta_{ei}), i = 1, 2, ..., n, \tag{1}$$

where the weight matrix $W_{ei} \in \mathbb{R}^{d\times p}$ and bias $\beta_{ei} \in R^{N\times p}$ are randomly initialised by corresponding dimensions, and the n groups of mapping feature nodes are concatenated into $Z^n \triangleq [Z_1, Z_2, ..., Z_n]$. Subsequently, using Z^n as input, the jth group of enhancement feature nodes is derived as:

$$H_j \triangleq \xi_j\left(Z^n W_{hj} + \beta_{hj}\right), j = 1, 2, ..., m, \tag{2}$$

where the weight matrix $W_{hj} \in \mathbb{R}^{np\times q}$ and bias $\beta_{hj} \in \mathbb{R}^{N\times q}$ are randomly initialised by corresponding dimensions, collectively denoted as $H^m \triangleq [H_1, H_2, ..., H_m]$. The mapping feature nodes and the enhancement feature nodes are concatenated to form the merged feature matrix A_n^m. The mapping between the input and output of IBLS can be expressed as:

$$Y = [Z^n \mid H^m]W_n^m = A_n^m W_n^m. \tag{3}$$

The ultimate output layer projects the fused features using a weight matrix $W_n^m \in \mathbb{R}^{(np+mq)\times c}$, thereby establishing the functional mapping from input to output.

2.2.2 | *Ridge Regression Algorithm*

The weights connecting the feature layer to the output layer in the flat network are derived through pseudoinverse computation, where mathematical approaches, including orthogonal projection, Gram–Schmidt orthogonalisation, iterative methods, and Singular Value Decomposition (SVD), are typically employed to calculate the generalised inverse. Nevertheless, these methods exhibit prohibitively computational demands when processing large-scale, high-dimensional training datasets. To address this limitation, we innovatively integrate a ridge regression-based algorithm within the proposed IBLS framework to optimise network weight computation, yielding notable advantages in training efficacy.

The top-layer weight optimisation is formulated as a regularised minimisation problem:

$$\arg\min : \|A_n^m W_n^m - Y\|_v^{\sigma_1} + \lambda \left\| W_n^m \right\|_u^{\sigma_2}, \tag{4}$$

where $\sigma_1, \sigma_2 > 0$ and u, v denote specified norm regularisers. Setting $\sigma_1 = \sigma_2 = 2$ with $u = v = 2$ (i.e., standard L2-norm regularisation) reduces this problem to ridge regression, whose closed-form solution approximates the Moore-Penrose pseudoinverse:

$$W_n^m = \left(\lambda I + AA^{\mathrm{T}}\right)^{-1} A^{\mathrm{T}} Y. \tag{5}$$

This solution differs from conventional ridge regression by explicitly constraining the Frobenius norm of the weight matrix (controlled by λ), where A^{T} is the transpose of A, λ the regularisation parameter, and I the identity matrix.

2.2.3 | *Incremental Learning for Incremental Data Based on IBLS*

For incrementally acquired training data $\{(X_a, Y_a)|X \in \mathbb{R}^{M\times d}, Y \in \mathbb{R}^{M\times c}\}$, the ith newly added group of mapping feature nodes is computed as:

$$Z_{Ii} \triangleq \phi_i(X_a W_{ei} + \beta_{ei}) \, (i = 1, 2, ..., n). \tag{6}$$

The n newly added groups of mapping feature nodes are concatenated into $Z_I^n \triangleq [Z_{I1}, Z_{I2}, ..., Z_{In}]$. Subsequently, using Z^n as input, the jth newly added group of enhancement nodes is derived as:

$$H_{Ij} \triangleq \xi_j\left(Z_I^n W_{hj} + \beta_{hj}\right) \, (j = 1, 2, ..., m). \tag{7}$$

The m newly added groups of enhancement nodes are concatenated into $H_I^m \triangleq [H_{I1}, H_{I2}, ..., H_{Im}]$.

Define $A_{In}^m \triangleq \left[Z_I^n \mid H_I^m\right]$ as the incremental merged feature matrix. The updated merged feature matrix is constructed as $\left(A_n^m\right)^* = \begin{bmatrix} A_n^m \\ \left(A_{\mathrm{In}}^m\right)^{\mathrm{T}} \end{bmatrix}$, whose pseudoinverse $\left(\left(A_n^m\right)^*\right)^+$ admits the recursive formulation:

$$\left(\left(A_n^m\right)^*\right)^+ = \left[\left(A_n^m\right)^+ - BD^{\mathrm{T}} | B\right], \tag{8}$$

where D^{T} and B^{T} are both derived from the relevant formulas of A_n^m and A_{In}^m. Specifically, $D^{\mathrm{T}} = \left(A_{In}^m\right)^{\mathrm{T}}\left(A_n^m\right)^+$

$$B^T = \begin{cases} \left(\left(A_{In}^m\right)^{\mathrm{T}} - D^{\mathrm{T}} A_n^m\right)^+, & \text{if} \left(A_{In}^m\right)^{\mathrm{T}} - D^{\mathrm{T}} A_n^m \neq 0 \\ \left(1 + D^{\mathrm{T}} D\right)^{-1}\left(A_n^m\right)^+ D, & \text{if} \left(A_{In}^m\right)^{\mathrm{T}} - D^{\mathrm{T}} A_n^m = 0 \end{cases}. \tag{9}$$

Therefore, the updated weights are

$$\left(W_n^m\right)^* = W_n^m + \left((Y_a)^{\mathrm{T}} - \left(A_{In}^m\right)^{\mathrm{T}} W_n^m\right)B, \tag{10}$$

where Y_a denotes the label matrix of incremental data.

Incremental learning substantially reduces computational overhead associated with weight updates, enabling efficient incorporation of new data into existing models. This approach is particularly advantageous for scenarios with continuously expanding datasets, circumventing the resource-intensive demands of full retraining.

2.3 | Knee Joint Moment Prediction Based on IBLS Framework

Within the IBLS framework, three motion-specific predictors are instantiated for level walking, stair ascent, and stair descent. During the training stage, each predictor is initially built as a generic model. We integrate IMU-derived multidimensional angle features from multiple subjects within the same locomotion mode. These features are then paired with joint moment labels to create a general dataset for offline training. To further enhance the model's ability to adapt to individual biomechanical differences, subject-specific incremental learning is performed using data from the target individual. This enables the model to rapidly incorporate personalised kinematic characteristics and achieve individualised adaptation. Finally, during inference, preprocessed IMU signals from the target subject are fed into the corresponding motion-specific predictor to generate the estimated knee joint moments.

3 | Results

This section provides a systematic description of the experimental framework and corresponding results supporting this study. We begin by utilising two high-quality, publicly available biomechanical datasets (Dataset A and Dataset B) as the foundation for all analyses. We then detail the experimental setup, including the computational hardware, model architectures, hyperparameter configurations, and regularisation strategies for the three representative predictors: IBLS, ANN, and LSTM. To rigorously evaluate model performance while minimising the risk of data leakage, we adopt leave-one-subject-out cross-validation and report Root Mean Squared Error (RMSE) and the Coefficient of Determination (R^2) as the primary quantitative metrics. Building upon this foundation, this section presents the design and outcomes of three key experimental components: (1) the IMU configuration selection experiment; (2) the performance comparison between IBLS and baseline models (ANN and LSTM); and (3) the comparison between increment and retraining for personalised model adaptation.

3.1 | Datasets

This study utilises two high quality publicly available biomechanical datasets to ensure comprehensive and reliable experimental evidence. Dataset A [39] encompasses multimodal recordings of 22 participants performing level walking at three self-selected speeds (0.88 ± 0.19 m/s for slow, 1.17 ± 0.21 m/s for normal, and 1.45 ± 0.27 m/s for fast), alongside stair ascent and descent across four step heights (102, 127, 152, and 178 mm) at self-selected velocities. Dataset B [40] includes data from 12 participants during level walking at three specified speeds (0.6, 1.2, and 1.8 m/s), as well as stair ascent and descent at a fixed height of 152 mm, performed at three self-selected velocities: slow, normal, and fast. Both datasets provide high-fidelity reference knee joint moments by integrating 200 Hz inertial measurement unit (IMU) signals with synchronised motion capture and force plate data, which were then down sampled to 200 Hz. The detailed information of the two datasets is summarised in Table 1. For both datasets, lower limb segment orientations and joint angles were computed from the IMU signals, and knee joint moments were obtained through OpenSim's inverse dynamics toolbox [41]. All data were subsequently standardised to ensure temporal alignment and label consistency, establishing a robust and reproducible foundation for the subsequent experiments.

3.2 | Model Implementation Details

Experiments were conducted on a workstation equipped with an Intel Core i9-13900HX processor, NVIDIA GeForce RTX 4060 Laptop GPU, and 32 GB RAM. The IBLS employed 10 mapping node groups (5 nodes/group, Sigmoid activation) and 10 enhancement node groups (5 nodes/group, Tanh activation); the ANN implemented three hidden layers (128–64–32 neurons, ReLU activation, dropout 0.2) trained for 100 epochs with a batch size of 32, a learning rate of 0.001, and Mean Squared Error (MSE) loss; the LSTM implemented one hidden layer (64 units, Tanh activation, dropout 0.2) trained for 100 epochs with a batch size of 32, a learning rate of 0.001, and MSE loss; the Transformer implemented a 4-layer architecture (8 attention heads, 128 dimensions, GRLU activation, dropout 0.2), identically trained for 100 epochs with a batch size of 32, a learning rate of 0.001, and MSE loss; the TCN-LSTM implemented 3 convolutional layers (64 filters, ReLU activation) and 1 LSTM layer (64 units, Tanh activation) with a dropout rate of 0.2, trained for 100 epochs with a batch size of 32, a learning rate of 0.001, and MSE loss, as summarised in Table 2.

To justify the chosen training schedules, the architectures and the relatively small number of epochs of the reasonable baselines (ANN and LSTM), as well as the Transformer and TCN-LSTM models, were determined based on the low intrinsic complexity and low-dimensional characteristics of the dataset in this study. We confirm that the baseline models were sufficiently optimised. Higher network dimensions or excessive epochs (unlike in typical deep learning studies) would directly lead to overfitting and performance saturation of the models. Furthermore, maintaining a relatively lightweight configuration across both the standard baselines and the advanced deep learning approaches ensures a fair comparison with the IBLS, particularly in terms of accuracy-efficiency trade-offs.

3.3 | Evaluation Protocol

Employing leave-one-subject-out (LOSO) cross-validation to mitigate data leakage risks, this study iteratively designates each sample as the test set while utilising the remainder for training, ensuring objective performance evaluation. For comprehensive model assessment, RMSE and R^2 are adopted below:

TABLE 1 | Information on Dataset A and Dataset B.

Indicator		Dataset A [39]	Dataset B [40]
Subjects	Number	22	12
	Age (year)	21 ± 3.4	21.8 ± 3.2
	Height (m)	1.70 ± 0.07	1.77 ± 0.08
	Mass (kg)	68.3 ± 10.83	76.9 ± 14.4
Level walking	Speeds (m/s)	0.88, 1.17, and 1.45	0.6, 1.2, and 1.8
Stair climbing	Stair height (mm)	102, 127, 152, and 178	152
	Speeds	Self-selected velocity	Slow, normal, and fast

TABLE 2 | Training details summary.

Models	Hidden layers (neurons)	Activation function	Dropout rate	Batch size	Learning rate	Epochs	Loss function
ANN	3 layers (128, 64, 32 neurons)	ReLU	0.2	32	0.001	100	MSE
LSTM	1 layer (64 units)	Tanh	0.2	32	0.001	100	MSE
Transformer	4 layers (8 heads, 128 dim)	GRLU	0.2	32	0.001	100	MSE
TCN-LSTM	3 conv layers (64 filters), 1 LSTM (64 units)	ReLU, Tanh	0.2	32	0.001	100	MSE
IBLS	10 map groups (5 nodes), 10 enh groups (5 nodes)	Sigmoid, Tanh	None	None	None	None	None

$$\mathrm{RMSE} = \sqrt{\frac{1}{n}\sum_{i=1}^{n}(y_i - \hat{y}_i)^2}, \tag{11}$$

$$R^2 = 1 - \frac{\sum_{i=1}^{n}(y_i - \hat{y}_i)^2}{\sum_{i=1}^{n}(y_i - \bar{y}_i)^2}, \tag{12}$$

where y_i and $\hat{y}_i$ represent actual and predicted moments, respectively, $\bar{y}_i$ denotes the mean of actual moments, and n represents the number of samples in the test set. RMSE quantifies the average deviation magnitude between predictions and ground truth (lower values indicate higher accuracy), while R^2 characterises the model's explanatory power for target variability (range [0, 1], with values approaching 1 reflecting superior goodness-of-fit), collectively establishing a multidimensional quantitative validation framework.

TABLE 3 | Specific configuration solutions.

Case		IMU configuration
1	Bilateral	2 thighs (B-T)
2		2 shanks (B-S)
3		2 thighs and 2 shanks (B-TS)
4		2 thighs, 2 shanks, and 2 feet (B-TSF)
5	Unilateral	1 thigh and 1 shank (U-TS)
6		1 thigh, 1 shank, and 1 foot (U-TSF)
Case		**Sliding time window size**
1		10 ms
2		50 ms
3		100 ms

3.4 | IMU Configuration Analysis

The IMU configurations in this work include all six solutions for capturing lower limb motion data, including both unilateral and bilateral configurations. The bilateral schemes include bilateral thigh-shank-foot (B-TSF) setup, bilateral thigh-shank (B-TS) setup, and bilateral thigh (B-T) setup, as well as bilateral shank (B-S) setup. The unilateral schemes include unilateral thigh-shank-foot (U-TSF) setup and unilateral thigh-shank (U-TS) setup. To balance real-time latency and temporal context, we adopt three causal sliding-window lengths: 10, 50, and 100 ms, with a 5 ms stride (i.e., one sample at the effective 200 Hz rate). Specifically, 10 ms targets high-frequency control loops (100–200 Hz) with minimal latency; 50 ms provides a more robust context while remaining responsive; 100 ms captures richer intra gait dynamics and yields the largest gains for unilateral/fewer sensor configurations, whereas bilateral multi IMU setups benefit less from longer windows because shorter windows already supply sufficient information. For example, when the sliding window length is 100 ms, the window contains 20 data points. The label corresponding to the last column of data points in each sliding window was used as the label for the entire sliding window data. Table 3 shows the specific configuration solutions.

Leveraging leave-one-out cross-validation (LOOCV) on two independent datasets (Dataset A and Dataset B), we quantitatively evaluate knee moment prediction efficacy across level walking, stair ascent, and descent for optimal IMU topology selection, where LOOCV validated RMSE and R^2 metrics across both datasets are visualised in Figures 2 and 3. Furthermore, representative samples (Subject A25 from Dataset A and Subject A02 from Dataset B) are selected to demonstrate prediction performance differences, with moment prediction fitting curves for three locomotor modes intuitively contrasting configuration effects as shown in Figures 4 and 5.

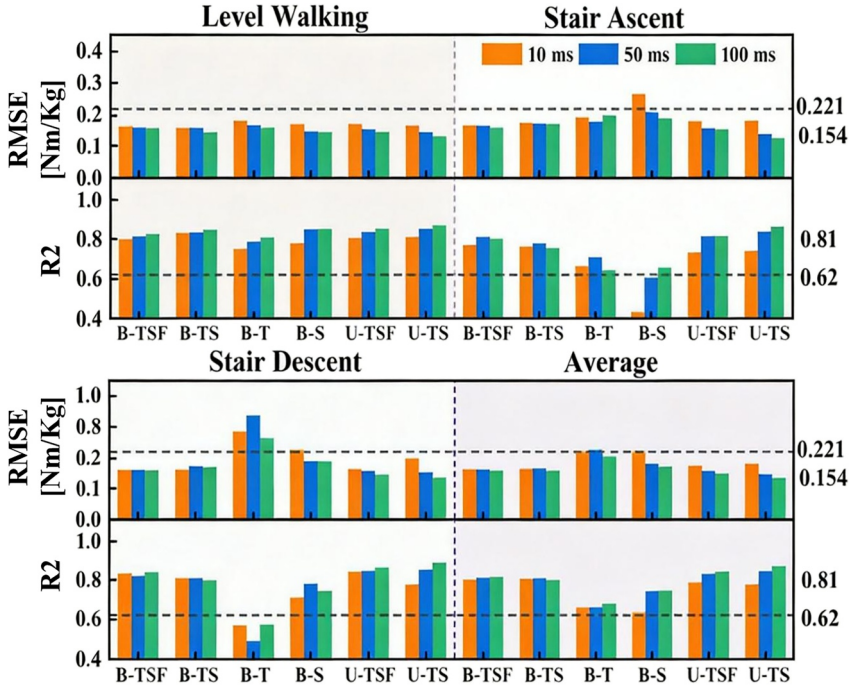


FIGURE 2 | The motion estimation performance evaluation of 18 configuration schemes combining different IMU placements and time windows for three motion types across two distinct datasets (Dataset A).

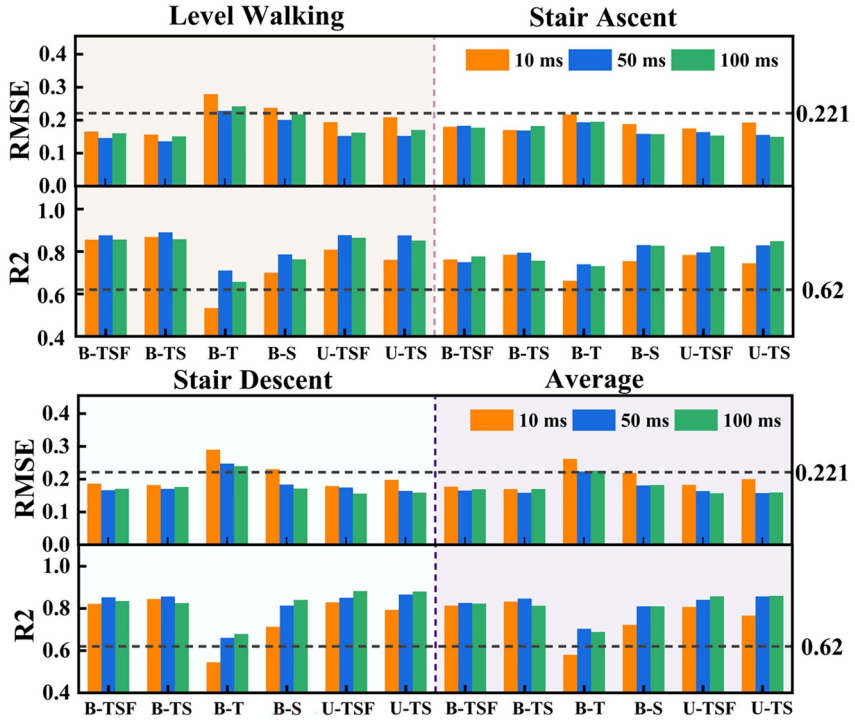


FIGURE 3 | The motion estimation performance evaluation of 18 configuration schemes combining different IMU placements and time windows for three motion types across two distinct datasets (Dataset B).

Following the tiered evaluation criteria established in [15], baseline level (RMSE = 0.221 Nm/kg and R^2 = 0.62)—experimental analysis reveals 13 IMU configurations simultaneously meeting baseline standards across both datasets during all three locomotion modes (level walking, stair ascent, and stair descent), including: (1) bilateral thigh-shank-foot configurations (10, 50, 100 ms time windows, totalling 3 variants), (2) bilateral thigh-shank configurations (10, 50, and 100 ms time windows, totalling 3 variants), (3) bilateral shank configuration (100 ms time window only, 1 variant), (4) unilateral thigh-shank-foot

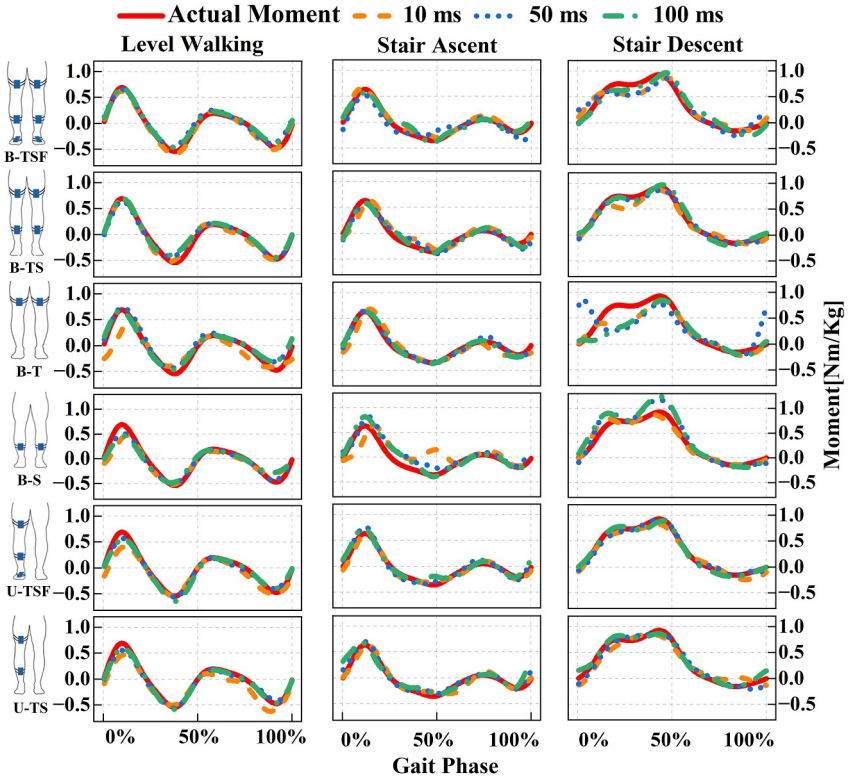


FIGURE 4 | Comparative knee joint moment fitting with IBLS across IMU placement topologies and temporal windows for level walking, stair ascent, and stair descent (Subject A25, Dataset A).

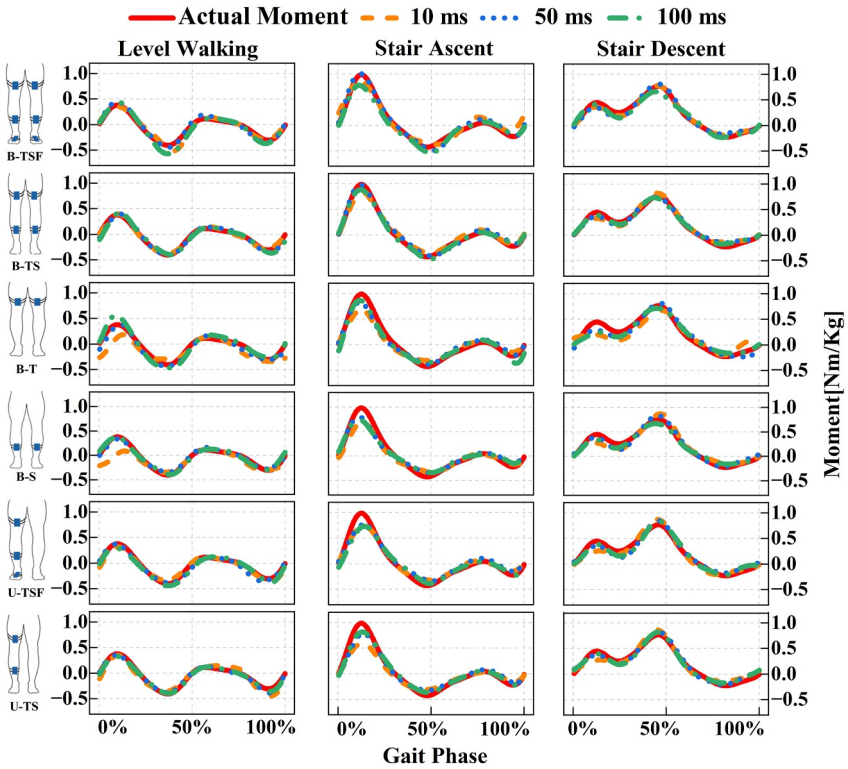


FIGURE 5 | Comparative knee joint moment fitting with IBLS across IMU placement topologies and temporal windows for level walking, stair ascent, and stair descent (Subject A02, Dataset B).

configurations (10, 50, and 100 ms time windows, totalling 3 variants), and (5) unilateral thigh-shank configurations (10, 50, and 100 time windows, totalling 3 variants).

The following observations can be made by analysing Figures 2 and 3. Both the bilateral thigh-shank-foot and bilateral thigh-shank configurations can maintain high prediction accuracy

using smaller window sizes with bilateral setups (e.g., 10 ms). This IMU setup is applicable to control applications that require high real-time performance and allow for bilateral wearing (e.g., bilateral exoskeletons). To address the potential drawbacks of reduced spatial information, both the unilateral thigh-shank-foot and unilateral thigh-shank configurations can only maintain high torque prediction accuracy using larger window sizes with unilateral setups (50 ms, 100 ms). This IMU setup is applicable to control applications that require lower real-time performance and only allow for unilateral wearing (e.g., unilateral exoskeletons). The bilateral shank configuration can only maintain high torque prediction accuracy under larger window sizes (50 ms, 100 ms). This IMU setup is applicable to control applications that require lower real-time performance and necessitate wearing IMUs on bilateral shanks. In contrast, as a potential drawback, the bilateral thigh configuration yields relatively low moment prediction accuracy under all time windows in the experiments.

Considering overall estimation accuracy, real-time performance, and sensor wearability, we identify the unilateral thigh-shank configuration (100 ms) as the optimal placement strategy in this study. Based on this optimised configuration, all subsequent comparative experiments and validation analyses were conducted under these conditions to ensure the consistency and comparability of research findings.

3.5 | Comparison With Existing Methods

To fully verify the comprehensive advantages of the IBLS model, a systematic performance comparison was conducted against standard baselines (ANN and LSTM) and advanced deep learning approaches (the Transformer and a cascaded TCN-LSTM network). This selection is motivated as follows: (1) ANN, a classical feed-forward universal approximator, serves as a strong regression baseline widely used in wearable sensing when temporal dependencies are not explicitly modelled; (2) LSTM, a representative sequence model, explicitly captures short- and long-term dependencies in IMU time series, serving as a robust baseline for joint moment prediction; (3) The Transformer, an advanced self-attention based model, effectively captures global dependencies in long IMU sequences, representing a cutting-edge approach for high-precision moment prediction; and (4) TCN-LSTM, an advanced cascaded architecture, synergises TCN's multiscale local feature extraction with LSTM's sequential dynamic modelling, making it highly effective for mapping complex joint dynamics from nonlinear multi-sensor data. Notably, consistent with the IBLS architecture, each comparative model (ANN, LSTM, Transformer, and TCN-LSTM) was implemented as a dedicated network trained separately for each locomotion mode (i.e., level walking, stair ascent, and stair descent). In other words, these comparative models replace only the IBLS component (c) in Figure 1, rather than employing a single generalised model for all motions. This fully ensures the fairness of the comparison. IBLS was evaluated alongside these four models under identical preprocessing, windowing, and LOOCV protocols. This experimental design ensured a fair assessment of accuracy, efficiency, and real-time performance while minimising bias towards any specific network architecture. Performance metrics for knee joint moment prediction were compared across all subjects in Datasets A and B. The evaluated locomotion modes included level walking, stair ascent, and stair descent. The average experimental results are presented in Table 4.

To visually illustrate the moment prediction results of the five models (IBLS, ANN, LSTM, Transformer, and TCN-LSTM), representative subjects A25 and A02 from Dataset A and Dataset B were selected as typical samples to generate the moment prediction plots (Figure 6).

Across three locomotion modes—level walking, stair ascent, and stair descent—the IBLS model demonstrated competitive prediction accuracy compared to the Transformer and TCN-LSTM models, while maintaining notable performance advantages over the ANN and the LSTM in RMSE and R^2. The following analysis focuses on the average prediction accuracy metrics. Specifically for Dataset A, compared to the ANN and LSTM, the IBLS model reduced the RMSE by 40.74% and 15.79%, while improving the R^2 by 18.92% and 4.76%, respectively. When compared to the TCN-LSTM, the IBLS model further reduced the RMSE by 5.88% and enhanced the R^2 by 2.33%. The Transformer model achieved peak performance in estimation precision, while the IBLS model demonstrated a near equivalent accuracy level. Compared to the Transformer, the IBLS model showed only a marginal RMSE increase of 6.67% and a slight R^2 reduction of 1.12%. Similar trends were observed in Dataset B. Compared to the ANN and LSTM, the IBLS model reduced the RMSE by 30.43% and 5.88%, while improving the R^2 by 24.64% and 4.88%, respectively. The IBLS model achieved an identical RMSE to that of the TCN-LSTM, while improving the R^2 by 2.38%. Compared to the Transformer, the RMSE of the IBLS model increased by only 6.67%, and its R^2 decreased by only 1.15%.

Leveraging the flattened architecture of the IBLS model and its pseudo inverse analytical solution training mechanism, the proposed model achieves notable computational efficiency improvements. The following analysis focuses on the average training time. Regarding standard baselines, on Dataset A, the IBLS model requires only 35.2% of the ANN's training time and just 7.2% of the LSTM's training time. For Dataset B, its training time is further reduced to 25.8% of the ANN's and 7.7% of the LSTM's. When evaluated against advanced deep learning approaches, this computational efficiency becomes even more pronounced. On Dataset A, the IBLS model requires only 3.9% of the Transformer's training time and a mere 3.3% of the TCN-LSTM's training time. For Dataset B, its training time is equivalent to just 3.5% of the Transformer's and 3.0% of the TCN-LSTM's. Consequently, these findings highlight the clear advantages of the IBLS model in minimising training latency for embedded exoskeleton applications.

3.6 | Incremental Learning Experiments

In applications such as human-robot interaction and wearable exoskeletons, the dynamic variability of movement patterns across individuals often limits the performance of generalised models. Moreover, traditional deep learning approaches rely on full-data retraining, causing computational complexity to scale linearly with data size and hindering the development of efficient personalised models. This section demonstrates the

TABLE 4 | Comparison of the performance of different moment estimation algorithms.

		Dataset A			Dataset B		
Activity	**Model**	**RMSE (Nm/Kg)**	R^2	**Training time (s)**	**RMSE (Nm/Kg)**	R^2	**Training time (s)**
Level walking	ANN	0.30	0.78	27.95	0.22	0.73	46.42
	LSTM	0.27	0.82	163.64	0.16	0.84	159.10
	Transformer	0.21	0.89	310.45	0.15	0.86	285.60
	TCN-LSTM	0.24	0.85	380.20	0.16	0.85	345.15
	IBLS (ours)	0.22	0.88	11.07	0.16	0.85	12.19
Stair ascent	ANN	0.30	0.66	46.82	0.20	0.75	48.58
	LSTM	0.14	0.83	228.12	0.16	0.82	170.74
	Transformer	0.12	0.87	420.15	0.14	0.86	380.40
	TCN-LSTM	0.13	0.85	490.80	0.15	0.84	430.25
	IBLS (ours)	0.13	0.85	17.08	0.15	0.85	12.80
Stair descent	ANN	0.19	0.79	49.95	0.28	0.59	42.01
	LSTM	0.15	0.86	217.73	0.18	0.81	129.76
	Transformer	0.12	0.92	394.50	0.16	0.88	355.20
	TCN-LSTM	0.14	0.88	465.30	0.17	0.83	410.80
	IBLS (ours)	0.13	0.91	15.75	0.17	0.87	10.40
Average	ANN	0.27	0.74	41.57	0.23	0.69	45.67
	LSTM	0.19	0.84	203.16	0.17	0.82	153.20
	Transformer	0.15	0.89	375.10	0.15	0.87	340.20
	TCN-LSTM	0.17	0.86	445.60	0.16	0.84	395.40
	IBLS (ours)	0.16	0.88	14.63	0.16	0.86	11.80

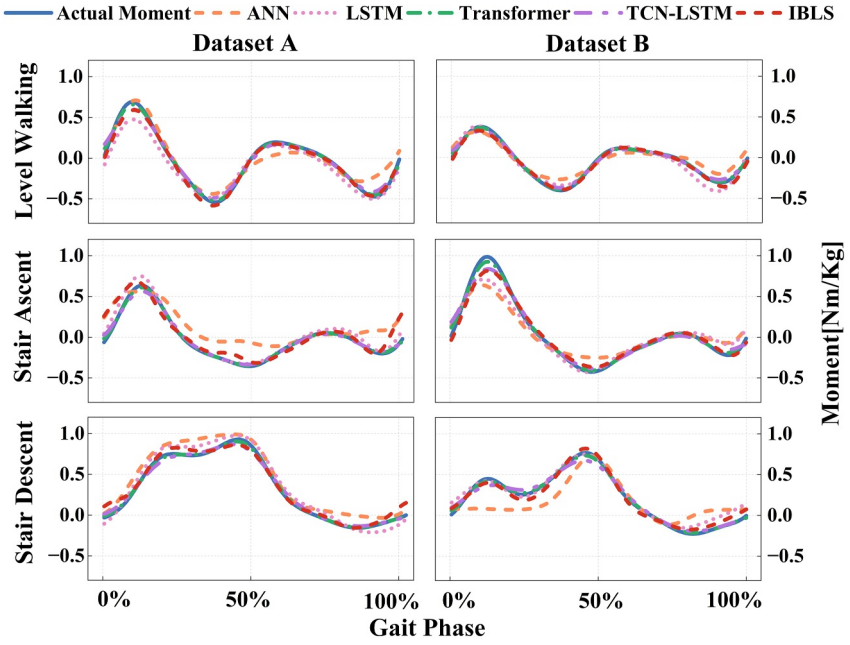


FIGURE 6 | Comparative analysis of knee moment prediction curves using multiple algorithms (ANN, LSTM, Transformer, TCN-LSTM and IBLS) across different gait modes (level walking, stair ascent, and stair descent), demonstrating predictive efficacy over one complete gait cycle. Dataset A displays the results for Subject A25, while Dataset B corresponds to Subject A02.

feasibility of using the IBLS incremental algorithm to construct personalised models, which notably reduces computational overhead compared to full retraining while maintaining comparable performance.

For each target subject in Dataset A and Dataset B, we first trained an 'original' model using data from all non-test subjects, serving as a generalised baseline without incremental updates. The non-test subset was then used as the source for subject-

specific incremental learning, which was performed through three sequential update stages (1st update, 2nd update, and 3rd update).

To explain how sensitive the incremental learning performance is to the size and selection of incremental data, the use of 10 gait cycles per update stage is systematically explained to establish an empirical balance between personalisation depth and computational efficiency. It is pointed out that utilising fewer cycles often fails to adequately capture the inherent intra-subject gait variability, resulting in insufficient weight updates and failing to yield meaningful personalisation. Conversely, while larger batches might further refine the model, they introduce unnecessary computational overhead, which contradicts the goal of rapid model adjustment. Therefore, 10 gait cycles were determined as a reasonable lower bound for effective adaptation. Regarding the selection of incremental data, in each iteration, 10 gait cycles from the same target subject were added, ensuring no overlap with the test set. The performance is summarised in Table 5 and Figure 7.

Analysis of composite locomotion mode metrics reveals: For Dataset A, the aggregated RMSE decreases to 0.1334 Nm/Kg after three incremental learning phases, representing an 18.86% reduction from the baseline model (0.1644), while the aggregated R^2 improves to 0.9176—a 5.70% increase over the baseline (0.8681). For Dataset B, the composite RMSE reaches 0.1004 Nm/Kg, demonstrating a substantial 42.96% decrease from the initial model (0.1760), and the composite R^2 rises to 0.9382, achieving a 13.25% enhancement over the initial value (0.8284). These results systematically affirm the efficacy of incremental learning in enhancing model predictive performance.

Experimental results indicate that incremental learning and full-data retraining achieve highly comparable prediction accuracy metrics (RMSE and R^2), and in certain cases, incremental learning even slightly outperforms full-data retraining. However, the incremental strategy achieves over a 60% reduction in training time compared with full retraining. Specifically for Dataset A, after three incremental learning phases, the composite training time decreases to 38.52%, 39.16%, and 39.82% of the full retraining baselines consecutively. For Dataset B, the corresponding phase-wise time consumption constitutes 43.95%, 41.86%, and 40.80% of baseline values. These findings validate that the incremental strategy reduces average training resource consumption by over 60% while maintaining equivalent prediction accuracy.

4 | Discussion

In this section, we first justify the fairness of our model comparisons against existing literature (Section 4.1), then provide a quantitative assessment of the computational efficiency for online deployment on embedded platforms (Section 4.2) and finally discuss the limitations of this study along with directions for future work (Section 4.3).

4.1 | Fairness of Model Comparison

For the datasets used in this paper (Dataset A and Dataset B), several studies have conducted knee joint moment prediction experiments using the same datasets. For Dataset A, the study by Hossain et al. [13] adopted the Kinetics-FM-DLR-EnsembleNet method, taking six-dimensional motion data collected from three IMU sensors placed on the thigh, shank, and foot as input, to build a general-purpose model covering multiple daily ambulation modes, including treadmill, level-ground, ramp, and stair walking. This method reported a normalised root mean square error (NRMSE) for knee joint moment ranging from 3.25% to 5.48%, with a training time of up to 20 h. The study by Molinaro et al. [26] proposed a task-agnostic exoskeleton controller, which used multimodal sensor data from the exoskeleton's onboard IMUs (thigh, shank, foot), joint encoders, and pressure insoles as input, to develop a general-purpose model for 28 cyclic, impedance-like, and unstructured daily activities (e.g., level walking, weight lifting, lateral cutting). The coefficient of determination (R^2) for knee joint moment prediction was 0.86 for cyclic activities and 0.87 for impedance-like activities. The study by Tang et al. [42] proposed the TCN-LSTM method, which took 24-dimensional motion signals from four six-axis IMUs (forefoot, lower leg, thigh, and trunk) as input, to build a task-specific model for gait. It achieved a mean absolute error (MAE) of 0.049 Nm/kg for knee joint moment prediction. For Dataset B, the study by Hur et al. [43] proposed a user-adaptive LSTM model, taking acceleration, gyroscope, and Euler angle data from eight IMUs (torso, pelvis, bilateral femurs, tibias, and calcanei) as input, to build a model for straight walking. It reported a root mean square error (RMSE) of approximately 5.5° for knee joint angle prediction.

The aforementioned studies differ significantly from the present work in terms of activity types, input variables, evaluation metrics, and even sensor hardware configurations. Consequently, direct cross-study comparisons cannot guarantee fairness. To ensure consistency and impartiality in the comparison,

TABLE 5 | Incremental learning versus retraining.

		Dataset A			Dataset B		
	Model	**RMSE (Nm/Kg)**	**R^2**	**Training time (s)**	**RMSE (Nm/Kg)**	**R^2**	**Training time (s)**
Original	Original	0.16	0.87	14.99	0.18	0.83	11.75
1st update	Retraining	0.15	0.89	16.90	0.14	0.88	13.58
	Increment	0.15	0.90	6.51	0.13	0.90	5.97
2nd update	Retraining	0.15	0.90	17.20	0.11	0.92	14.87
	Increment	0.14	0.90	6.73	0.11	0.92	6.22
3rd update	Retraining	0.14	0.91	17.49	0.10	0.93	16.18
	Increment	0.13	0.92	6.96	0.10	0.94	6.60

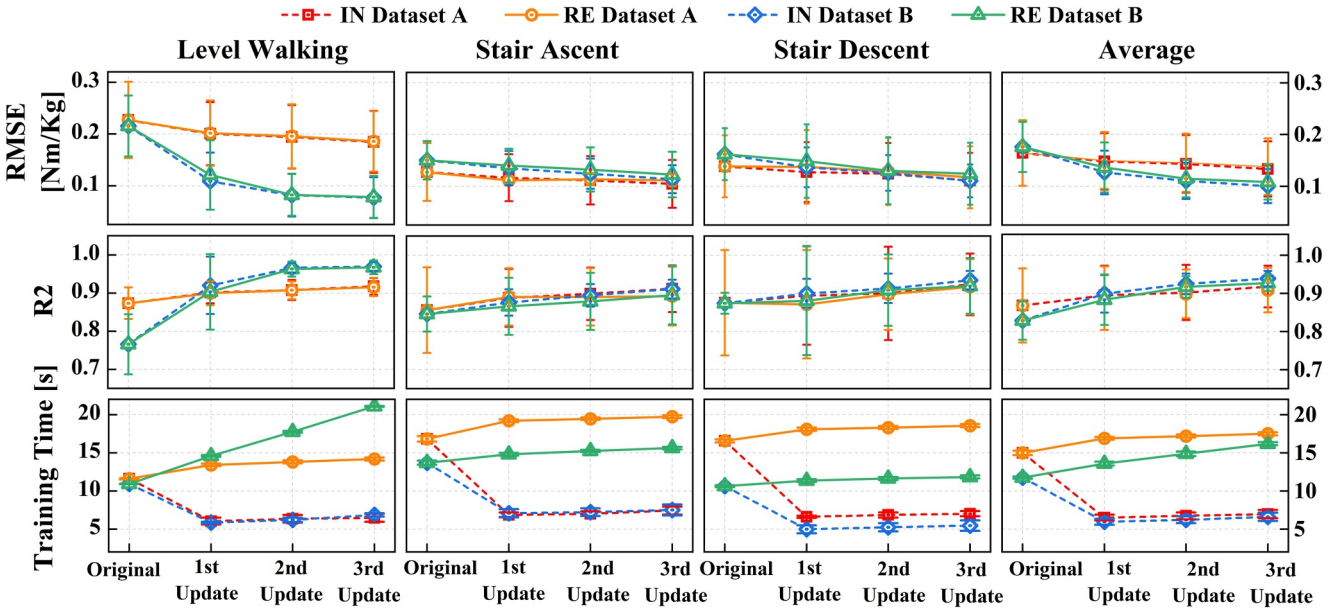


FIGURE 7 | Comparative experimental analysis of incremental learning versus full-data retraining efficacy across datasets under three gait modes: level walking, stair ascent, and stair descent. By iteratively injecting non-test subsets from target subjects as incremental data sources during phased training, this experiment systematically compares RMSE, R^2, and training time metrics. The results demonstrate that the incremental learning strategy achieves over 60% average reduction in training resource consumption while maintaining prediction accuracy comparable to full-data retraining.

we locally reproduced and evaluated several models, including ANN, LSTM, Transformer, and TCN-LSTM, with the detailed results presented in Section 3.5. All compared models strictly adhered to the same training paradigm as IBLS, namely training task-specific neural networks for individual activities rather than employing a single general-purpose model to handle all activities. Specifically, these models only replaced the IBLS network structure in Figure 1c and were trained as dedicated subnetworks for three distinct activities: level walking, stair ascent, and stair descent. Under this fair setting, the experimental results conclusively demonstrate the superiority of the IBLS method.

4.2 | Analysis of Computational Efficiency for Online Deployment

As an additional discussion to elucidate the practical suitability for real-time and wearable robotics applications, quantitative estimates of inference latency and computational load during online deployment were first calculated on an Intel Core i9 testbed, yielding an average inference latency of 0.02 ms and an incremental update time of 6.5-s. In realistic wearable applications, however, control algorithms are deployed on embedded microcontrollers. Given the ultra-lightweight architecture of the proposed model, inference can be executed on a standard Cortex-M4/M7 MCU equipped with an FPU with an inference latency of less than 0.2 ms. This microsecond-level latency comfortably satisfies the strict 100–1000 Hz real-time control constraints required for joint actuation.

Furthermore, while the heavier computational load when incremental updates are triggered is challenging for a standalone MCU, it can be efficiently handled using a hierarchical control paradigm. The 6.5-s incremental update can be processed in the background by a high-level wearable edge processor. Upon completion, the compact updated weight matrices are swiftly transmitted to the low-level MCU via a communication bus. This architecture ensures continuous, high-frequency real-time inference while allowing the system to periodically adapt to dynamic user states without offline retraining.

4.3 | Limitations and Future Work

To acknowledge a notable limitation of this study, all experiments are conducted on datasets comprising healthy young adults in controlled laboratory conditions, without involving pathological gait populations (e.g., osteoarthritis, stroke, or amputees). As preliminary insights into how we anticipate the IBLS framework performing on such patients, the personalised joint moment prediction method proposed in this research demonstrates theoretical superiority. The gait of patients typically deviates significantly from that of healthy individuals, and the inter-subject variability may be substantially higher. If a generic model is employed to predict the moments of patients, the results will deviate significantly from the true values. Therefore, a personalised joint moment prediction scheme is crucial for patients. By performing incremental learning on patient-specific gait information based on a generic model, a moment prediction model tailored to a specific patient can be obtained, thereby achieving more accurate moment predictions. In future work, we will focus on applying this method to pathological gait populations.

It should be particularly noted that the primary focus of this work is to validate the feasibility and advantages of the IBLS method for joint moment estimation. To this end, the networks trained herein are dedicated predictors for individual locomotion modes and have not yet achieved unified modelling across multiple activities. This design inherently presents certain

limitations at the current stage. Therefore, an important direction for future research is to deeply integrate the gait classification module (illustrated in Figure 1b) with the single-activity prediction networks, thereby enabling moment estimation in multiactivity scenarios and supporting more complex locomotor tasks in real-world environments.

5 | Conclusion

This work addresses the dual challenges of computational efficiency and personalisation in data-driven knee joint moment estimation. We have developed and validated a novel framework based on the Incremental Broad Learning System (IBLS), which establishes a practical and efficient paradigm for personalised biomechanical modelling.

The principal contribution of this study is two-fold. First, the IBLS framework fundamentally redefines the training paradigm by substituting the iterative gradient descent of deep networks with a flattened architecture and an analytical ridge regression solver. Experimental results demonstrate that our approach yields higher prediction accuracy than standard ANN and LSTM baselines, while remaining highly competitive with advanced architectures like the Transformer and a cascaded TCN-LSTM network. This process leads to a reduction in training time: the training time for IBLS is approximately 30%, 7.5%, and 3.5% of the time required for ANN, LSTM, and the advanced models (Transformer and TCN-LSTM), respectively. Second, the framework inherently supports efficient personalisation. Its incremental learning algorithm enables rapid model adaptation to new individuals, reducing the computational cost of updates by over 60% compared to full model retraining. This capability effectively bridges the gap between a generalisable base model and subject-specific calibration, making on-demand personalisation feasible for real-world applications.

Beyond the algorithmic advance, our systematic sensor analysis provides actionable engineering guidance. We identified that a unilateral thigh-shank configuration with a 100 ms temporal window delivers performance comparable to more complex bilateral setups. This finding demonstrates that extended temporal context can compensate for reduced spatial sensing, offering a pathway to design simpler, more wearable, and user-friendly sensing systems without significant performance loss.

In summary, this research presents a notable step towards practical, user-centred biomechanical monitoring. By simultaneously solving critical problems of training efficiency and personalised adaptation, the proposed IBLS framework lays a foundational methodology for the next generation of intelligent, responsive, and efficient wearable assistive technologies.

Acknowledgements

The authors have nothing to report.

Funding

This work was supported in part by National Natural Science Foundation of China under Grants 62373016 and 62403020, in part by Beijing Natural Science Foundation Project under Grant 4262038, and in part by Zhiyuan Laboratory under Grant ZYL2025012.

Conflicts of Interest

The authors declare no conflicts of interest.

Data Availability Statement

The data that support the findings of this study are openly available in Dataset A: https://www.sciencedirect.com/science/article/abs/pii/S0021929021001007, Dataset B: https://www.nature.com/articles/s41597-023-02840-6.

References

1. W. L. Kenney, J. H. Wilmore, and D. L. Costill, *Physiology of Sport and Exercise* (Human Kinetics, 2021).

2. C. Wang, P. P. Chan, B. M. Lam, et al., "Real-Time Estimation of Knee Adduction Moment for Gait Retraining in Patients With Knee Osteoarthritis," *IEEE Transactions on Neural Systems and Rehabilitation Engineering* 28, no. 4 (2020): 888–894, https://doi.org/10.1109/tnsre.2020.2978537.

3. J.-H. Kim, S.-M. Lee, H.-S. Shin, et al., "Biomechanical Mechanisms Behind the Reduction of Knee Adduction Moment in Medial Knee Thrust Gait," *Scientific Reports* 15, no. 1 (2025): 37317, https://doi.org/10.1038/s41598-025-21220-1.

4. N. D. Reeves and F. L. Bowling, "Conservative Biomechanical Strategies for Knee Osteoarthritis," *Nature Reviews Rheumatology* 7, no. 2 (2011): 113–122, https://doi.org/10.1038/nrrheum.2010.212.

5. B. Jackson, A. Wluka, A. Teichtahl, M. E. Morris, and F. M. Cicuttini, "Reviewing Knee Osteoarthritis—A Biomechanical Perspective," *Journal of Science and Medicine in Sport* 7, no. 3 (2004): 347–357, https://doi.org/10.1016/s1440-2440(04)80030-6.

6. D. D. Molinaro, I. Kang, and A. J. Young, "Estimating Human Joint Moments Unifies Exoskeleton Control, Reducing User Effort," *Science Robotics* 9, no. 88 (2024): eadi8852, https://doi.org/10.1126/scirobotics.adi8852.

7. G. M. Gasparri, J. Luque, and Z. F. Lerner, "Proportional Joint Moment Control for Instantaneously Adaptive Ankle Exoskeleton Assistance," *IEEE Transactions on Neural Systems and Rehabilitation Engineering* 27, no. 4 (2019): 751–759, https://doi.org/10.1109/tnsre.2019.2905979.

8. T.-H. Huang, S. Zhang, S. Yu, et al., "Modeling and Stiffness-Based Continuous Torque Control of Lightweight Quasi-Direct-Drive Knee Exoskeletons for Versatile Walking Assistance," *IEEE Transactions on Robotics* 38, no. 3 (2022): 1442–1459, https://doi.org/10.1109/tro.2022.3170287.

9. X. Wu, A. Zhu, X. Wang, X. Ma, H. Mao, and J. Song, "Real-Time Gait Symmetry Enhancement in People With Unilateral Knee Injuries Using Deep Learning for Modulation of Knee Exoskeleton," in *2023 International Conference on Design Science (ICDS)* (IEEE, 2023), 1–7.

10. W. Meng, Z. Tian, C. Zhu, Q. Ai, and Q. Liu, "Optimized Impedance Control of a Lightweight Gait Rehabilitation Exoskeleton Based on Accurate Knee Joint Torque Estimation," *IEEE Transactions on Medical Robotics and Bionics* 6, no. 4 (2024): 1648–1657, https://doi.org/10.1109/tmrb.2024.3464671.

11. J. Zhang, P. Fiers, K. A. Witte, et al., "Human-in-the-Loop Optimization of Exoskeleton Assistance During Walking," *Science* 356, no. 6344 (2017): 1280–1284, https://doi.org/10.1126/science.aal5054.

12. Y. Ding, M. Kim, S. Kuindersma, and C. J. Walsh, "Human-in-the-Loop Optimization of Hip Assistance With a Soft Exosuit During

Walking," *Science Robotics* 3, no. 15 (2018): eaar5438, https://doi.org/10.1126/scirobotics.aar5438.

13. M. S. B. Hossain, Z. Guo, and H. Choi, "Estimation of Lower Extremity Joint Moments and 3d Ground Reaction Forces Using Imu Sensors in Multiple Walking Conditions: A Deep Learning Approach," *IEEE Journal of Biomedical and Health Informatics* 27, no. 6 (2023): 2829–2840, https://doi.org/10.1109/jbhi.2023.3262164.

14. H. Lim, B. Kim, and S. Park, "Prediction of Lower Limb Kinetics and Kinematics During Walking by a Single IMU on the Lower Back Using Machine Learning," *Sensors* 20, no. 1 (2019): 130, https://doi.org/10.3390/s20010130.

15. K. L. Scherpereel, D. D. Molinaro, M. K. Shepherd, O. T. Inan, and A. J. Young, "Improving Biological Joint Moment Estimation During Real-World Tasks With EMG and Instrumented Insoles," *IEEE Transactions on Biomedical Engineering* 71, no. 9 (2024): 2718–2727, https://doi.org/10.1109/tbme.2024.3388874.

16. L. Zhang, Z. Li, Y. Hu, C. Smith, E. M. G. Farewik, and R. Wang, "Ankle Joint Torque Estimation Using an EMG-Driven Neuromusculoskeletal Model and an Artificial Neural Network Model," *IEEE Transactions on Automation Science and Engineering* 18, no. 2 (2020): 564–573, https://doi.org/10.1109/tase.2020.3033664.

17. N. Hondo and T. Tsuji, "Torque Estimation of Knee Flexion and Extension Movements From a Mechanomyogram of the Femoral Muscle," *IEEE Transactions on Neural Systems and Rehabilitation Engineering* 30 (2022): 1120–1126, https://doi.org/10.1109/tnsre.2022.3169225.

18. L. Zhang, D. Soselia, R. Wang, and E. M. Gutierrez-Farewik, "Estimation of Joint Torque by EMG-Driven Neuromusculoskeletal Models and LSTM Networks," *IEEE Transactions on Neural Systems and Rehabilitation Engineering* 31 (2023): 3722–3731, https://doi.org/10.1109/tnsre.2023.3315373.

19. L. Zhang, D. Soselia, R. Wang, and E. M. Gutierrez-Farewik, "Lower-Limb Joint Torque Prediction Using LSTM Neural Networks and Transfer Learning," *IEEE Transactions on Neural Systems and Rehabilitation Engineering* 30 (2022): 600–609, https://doi.org/10.1109/tnsre.2022.3156786.

20. W. Niu, Q. Bian, L. Yang, H. Zhou, and Z. Ding, "Cross-LSTM: Integrating Cross Attention With Long Short-Term Memory Neural Networks in Estimating Joint Moments From Wearable Sensors," *IEEE Transactions on Neural Systems and Rehabilitation Engineering* 33 (2025): 3793–3804, https://doi.org/10.1109/TNSRE.2025.3610281.

21. H. J. Bennett, K. Estler, K. Valenzuela, and J. T. Weinhandl, "Predicting Knee Joint Contact Forces During Normal Walking Using Kinematic Inputs With a Long-Short Term Neural Network," *Journal of Biomechanical Engineering* 146, no. 8 (2024): 081004, https://doi.org/10.1115/1.4064550.

22. J. Zhang, Y. Zhao, F. Shone, et al., "Physics-Informed Deep Learning for Musculoskeletal Modeling: Predicting Muscle Forces and Joint Kinematics From Surface EMG," *IEEE Transactions on Neural Systems and Rehabilitation Engineering* 31 (2022): 484–493, https://doi.org/10.1109/tnsre.2022.3226860.

23. Z. Wang, C. Chen, H. Chen, Y. Zhou, X. Wang, and X. Wu, "Dual Transformer Network for Predicting Joint Angles and Torques From Multi-Channel EMG Signals in the Lower Limbs," *IEEE Journal of Biomedical and Health Informatics* (2025), https://doi.org/10.1109/JBHI.2025.3555255.

24. B. Xiong, Y. Chang, N. Zeng, et al., "TranSEMG: A Trans-Scale Hybrid Model for High-Accurate Hip Joint Moment Prediction," *IEEE Transactions on Instrumentation and Measurement* 73 (2024): 1–11, https://doi.org/10.1109/tim.2024.3384565.

25. Z. Feng, D. Zhu, T. Wu, H. Li, and T. Han, "Self-Aware Fusion IMU-EMG Attention Dependence for Knee Adduction Moment Estimation During Walking," *IEEE Journal of Biomedical and Health Informatics* 6, no. 4 (2025): 1648–1657, https://doi.org/10.1109/JBHI.2025.3564981.

26. D. D. Molinaro, K. L. Scherpereel, E. B. Schonhaut, G. Evangelopoulos, M. K. Shepherd, and A. J. Young, "Task-Agnostic Exoskeleton Control via Biological Joint Moment Estimation," *Nature* 635, no. 8038 (2024): 337–344, https://doi.org/10.1038/s41586-024-08157-7.

27. D. D. Molinaro, I. Kang, J. Camargo, M. C. Gombolay, and A. J. Young, "Subject-Independent, Biological Hip Moment Estimation During Multimodal Overground Ambulation Using Deep Learning," *IEEE Transactions on Medical Robotics and Bionics* 4, no. 1 (2022): 219–229, https://doi.org/10.1109/tmrb.2022.3144025.

28. C. P. Chen, Z. Liu, and S. Feng, "Universal Approximation Capability of Broad Learning System and Its Structural Variations," *IEEE Transactions on Neural Networks and Learning Systems* 30, no. 4 (2018): 1191–1204, https://doi.org/10.1109/tnnls.2018.2866622.

29. C. P. Chen and Z. Liu, "Broad Learning System: An Effective and Efficient Incremental Learning System Without the Need for Deep Architecture," *IEEE Transactions on Neural Networks and Learning Systems* 29, no. 1 (2017): 10–24, https://doi.org/10.1109/tnnls.2017.2716952.

30. Z. Liu, C. P. Chen, S. Feng, Q. Feng, and T. Zhang, "Stacked Broad Learning System: From Incremental Flatted Structure to Deep Model," *IEEE Transactions on Systems, Man, and Cybernetics: Systems* 51, no. 1 (2020): 209–222, https://doi.org/10.1109/tsmc.2020.3043147.

31. L. Zhang, J. Li, G. Lu, et al., "Analysis and Variants of Broad Learning System," *IEEE Transactions on Systems, Man, and Cybernetics: Systems* 52, no. 1 (2020): 334–344, https://doi.org/10.1109/tsmc.2020.2995205.

32. H. Huang, T. Zhang, C. Yang, and C. P. Chen, "Motor Learning and Generalization Using Broad Learning Adaptive Neural Control," *IEEE Transactions on Industrial Electronics* 67, no. 10 (2019): 8608–8617, https://doi.org/10.1109/tie.2019.2950853.

33. S. Xu, J. Liu, C. Yang, X. Wu, and T. Xu, "A Learning-Based Stable Servo Control Strategy Using Broad Learning System Applied for Microrobotic Control," *IEEE Transactions on Cybernetics* 52, no. 12 (2021): 13727–13737, https://doi.org/10.1109/tcyb.2021.3121080.

34. S. Xu, T. Xu, D. Li, C. Yang, C. Huang, and X. Wu, "A Robot Motion Learning Method Using Broad Learning System Verified by Small-Scale Fish-Like Robot," *IEEE Transactions on Cybernetics* 53, no. 9 (2023): 6053–6065, https://doi.org/10.1109/tcyb.2023.3269773.

35. Y. Cao, M. Jia, P. Ding, X. Zhao, and Y. Ding, "Incremental Learning for Remaining Useful Life Prediction via Temporal Cascade Broad Learning System With Newly Acquired Data," *IEEE Transactions on Industrial Informatics* 19, no. 4 (2023): 6234–6245, https://doi.org/10.1109/tii.2022.3201977.

36. T. Xu, G. Han, H. Zhu, C. Lin, and J. Peng, "Multiscale BLS-Based Lightweight Prediction Model for Remaining Useful Life of Aero-Engine," *IEEE Transactions on Reliability* 73, no. 4 (2024): 1757–1767, https://doi.org/10.1109/tr.2023.3349201.

37. C. Zhu, Y. Pu, Z. Lyu, K. Yang, and Q. Yang, "Multidimensional Information Fusion and Broad Learning System-Based Condition Recognition for Energy Pipeline Safety," *Knowledge-Based Systems* 300 (2024): 112259, https://doi.org/10.1016/j.knosys.2024.112259.

38. X. Xu, S. Bao, H. Shao, and P. Shi, "A Multi Sensor Fused Incremental Broad Learning With DS Theory for Online Fault Diagnosis of Rotating Machinery," *Advanced Engineering Informatics* 60 (2024): 102419, https://doi.org/10.1016/j.aei.2024.102419.

39. J. Camargo, A. Ramanathan, W. Flanagan, and A. Young, "A Comprehensive, Open-Source Dataset of Lower Limb Biomechanics in Multiple Conditions of Stairs, Ramps, and Level-Ground Ambulation and Transitions," *Journal of Biomechanics* 119 (2021): 110320, https://doi.org/10.1016/j.jbiomech.2021.110320.

40. K. Scherpereel, D. Molinaro, O. Inan, M. Shepherd, and A. Young, "A Human Lower-Limb Biomechanics and Wearable Sensors Dataset During Cyclic and Non-Cyclic Activities," *Scientific Data* 10, no. 1 (2023): 924, https://doi.org/10.1038/s41597-023-02840-6.

41. A. Seth, M. Sherman, J. A. Reinbolt, and S. L. Delp, "OpenSim: A Musculoskeletal Modeling and Simulation Framework for in Silico Investigations and Exchange," *Procedia IUTAM* 2 (2011): 212–232, https://doi.org/10.1016/j.piutam.2011.04.021.

42. Z. Tang, Y. Wang, S. Mao, and D. Wei, "TCN-xLSTM: A Hybrid Temporal Model Integrating TCN and xLSTM for Lower Limb Joint Moment Estimation From IMU Signals," *IEEE Robotics and Automation Letters* 11, no. 1 (2025): 153–160, https://doi.org/10.1109/lra.2025.3632757.

43. B. Hur, S. Baek, I. Kang, and D. Kim, "Learning Based Lower Limb Joint Kinematic Estimation Using Open Source IMU Data," *Scientific Reports* 15, no. 1 (2025): 5287, https://doi.org/10.1038/s41598-025-89716-4.